Targeting the rich conformational landscape of *N*-allylmethylamine using rotational spectroscopy and quantum mechanical calculations

Weslley G. D. P. Silva, Tamanna Poonia and Professor Jennifer van Wijngaarden*

Department of Chemistry, University of Manitoba, Winnipeg, Manitoba, R3T 2N2, Canada

*Corresponding author

Email: vanwijng@cc.umanitoba.ca

Phone: (204)474-8379

Fax: (204)474-7608

Abstract

The highly variable conformational landscape of *N*-allylmethylamine (AMA) was investigated using Fourier transform microwave spectroscopy aided by high-level theoretical calculations to understand the energy relationship governing the interconversion between nine stable conformers. Spectroscopically, transitions belonging to four low energy conformers were identified and their hyperfine patterns owing to the ^{14}N quadrupolar nucleus were unambiguously resolved. The rotational spectrum of the global minimum geometry, conformer I, shows an additional splitting associated with a tunneling motion through an energy barrier interconnecting its enantiomeric forms. A two-step tunneling trajectory is proposed by finding transition state structures corresponding to the allyl torsion and NH inversion. Natural bond orbital and non-covalent interaction analyses reveal that an interplay between steric and hyperconjugative effects rules the conformational preferences of AMA.

Introduction

Amines are ubiquitous in nature. In biological media, for instance, the amino group is a key component in peptides, neurotransmitters and nucleosides, while in the atmosphere and interstellar medium (ISM), amino containing molecules are known participants in the chemistry of aerosols and evolution of stars, respectively.[1,2] In astrochemistry, amines are of great interest as potential precursors for the formation of amino acids and peptides under astrophysical conditions.[3,4] Prebiotic aminoacetonitrile (H_2NCH_2CN)[5] and methylamine (CH_3NH_2)[6,7], for example, are suggested to play a role

in the formation of the simplest amino acid glycine.[3,4] Although amino acids and peptides are well-known in biological environments, none have been unequivocally detected in the ISM making the hunt for a connection which links biology and astronomy an open scientific pursuit of significant importance. The careful study of additional nitrogen containing molecules that may lead to direct astronomical detections, or to laboratory synthesis of potential astrochemical targets, is therefore central to advance our understanding of the chemistry of the ISM.

Previous gas phase pyrolysis reports using allyl containing precursors, such as *N*-allylmethylamine (AMA, $H_2C{=}CH{-}CH_2{-}NH{-}CH_3$) and its oxygen and sulfur counterparts,[8,9] have shown that the thermal decomposition of this class of compounds led to the formation of species of astrochemical and atmospheric interest. In the case of AMA,[8] the main kinetically favored products at temperatures of 602–694K are propylene (CH_2CHCH_3)[10] and methanimine (CH_2NH)[11] which are known prebiotic molecules found in the TMC-1 and Sagittarius B2 molecular clouds, respectively.[2,8] This suggests that AMA is a good candidate to form novel molecular species which can then be characterized by rotational spectroscopy under laboratory conditions. Before understanding the products and processes in which AMA participates, a complete characterization of its conformational landscape, spectroscopic fingerprints and internal motions is compulsory.

Allyl derivatives of the type $H_2C{=}CH{-}CH_2{-}X$ tend to show a diverse conformational behavior which arises from internal rotations around its two single bonds.[12–14] Depending on the nature of the X substituent, a variety of effects, including steric hindrance, London dispersive forces and hydrogen bonding, can rule their conformational preferences. One

example is the many theoretical[14] and experimental[15–19] investigations required to partially understand the relative energy ordering of the four observed conformers of allylamine (H_2C=CH–CH_2–NH_2). For AMA, a previous low-resolution rotational spectroscopic study[20] at dry-ice temperature identified one rotamer which was attributed to the global minimum. This geometry was assumed to be at least 3.0 kJ mol^{-1} more stable than any other conformer due to an intramolecular hydrogen bond between the allyl and amino groups. At that time, no quantum mechanical calculations were performed to verify this and due to experimental limitations, the hyperfine structure owing to the ^{14}N quadrupolar nucleus and internal motions were not resolved.

Herein, we investigate the rich conformational space of AMA using modern Fourier transform microwave (FTMW) spectroscopy aided by density functional theory (DFT) and *ab initio* quantum mechanical calculations. Transitions from four unique conformations were observed in the rotational spectrum and their characteristic hyperfine splittings due to the ^{14}N quadrupolar nucleus were assigned. To understand the effects governing the conformational preferences, natural bond orbital (NBO)[21] and non-covalent interaction (NCI)[22] analyses were invoked. The results define the underlying factors that govern the conformational stability of AMA which will guide spectroscopic investigations in other regions of the electromagnetic spectrum.

Results

Conformational Searches

The conformational landscape of AMA was computationally explored using a joint approach involving molecular dynamics and high-level quantum mechanical calculations. A conformational search using the molecular dynamics GFN2-xTB method led to 17 possible geometries while the construction of a potential energy surface (PES) obtained at the B3LYP-D3(BJ)/cc-pVTZ level (Figure 1) located nine energy minima. The diversity of conformers found by both methods arise from internal rotations about the δ (C1=C2–C3–N) and θ (C2–C3–N–C4) dihedral angles (Figure 1). All possible minima were subjected to optimization and harmonic frequency calculations at the B3LYP-D3(BJ), B2PLYP-D3(BJ) and MP2 levels with the aug-cc-pVTZ basis set.

The results from the three levels of quantum chemical theory converge to yield nine unique energy minima—their geometries are similar to the ones located in the PES—whose natures are confirmed by the absence of imaginary frequencies. This is consistent with the hypothetical geometries from the assumption that the total number of unique conformers is 3^n (3^2= 9) with being n the number of dihedral angles which lead to different conformations. Pictorial representations of the nine optimized geometries of AMA are shown in Figure 1 while their Cartesian coordinates are provided in the supporting information (SI) file. Relative electronic energies with zero-point energy (ZPE) corrections and spectroscopic parameters for the nine stable conformers of AMA obtained at the B2PLYP-D3(BJ) and MP2 methods are given in Table 1, whereas the results from B3LYP-D3(BJ) are provided in the SI (Table S12) for comparison. The conformers are labeled using Roman numerals from I–IX which represent their order of stability in MP2

being I the most stable conformer. Overall, although the conformational energy ordering and predicted spectroscopic constants from the three different levels of theory are consistent with each other, the rotational constants from B2PLYP-D3(BJ) presented a better match with the experimentally determined values (Table S14).

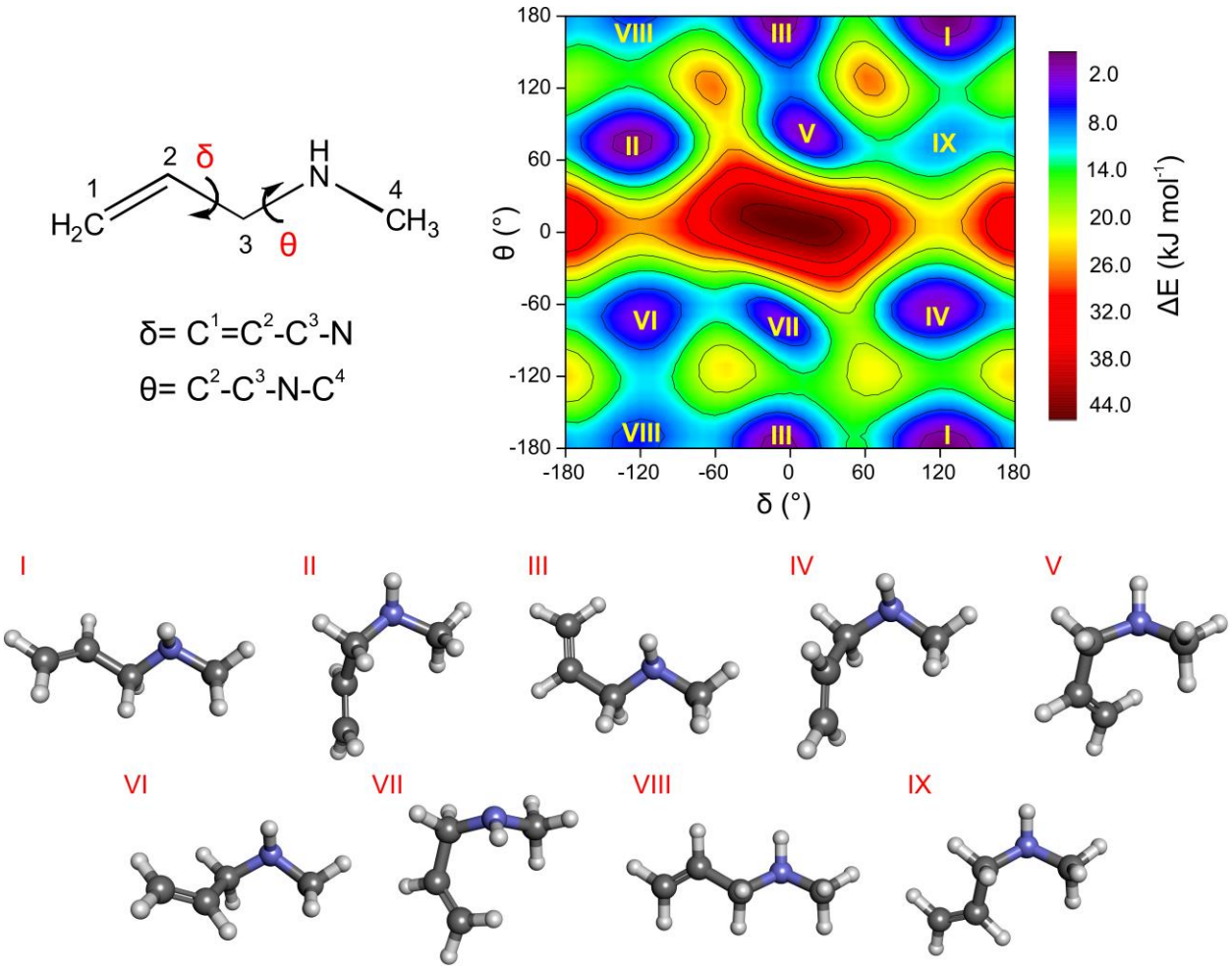

Figure 1. Potential energy surface (B3LYP-D3(BJ)/cc-pVTZ) and nine optimized conformers of AMA (B2PLYP-D3(BJ)/aug-cc-pVTZ) which arise through rotations around its δ and θ dihedral angles

Table 1. Calculated energies with zero-point (ZPE) corrections in kJ mol^{-1}, populations at 298K in %, electric dipole moment components in Debye and rotational constants in MHz for the nine conformers of AMA obtained using the B2PLYP-D3(BJ) and MP2 methods with the aug-cc-pVTZ basis set

Conformer	B2PLYP-D3(BJ)				MP2			
	ΔE_{ZPE}	*P*	*A*/*B*/*C*	$\lvert\mu_a\rvert$/ $\lvert\mu_b\rvert$/ $\lvert\mu_c\rvert$	ΔE_{ZPE}	*P*	*A*/*B*/*C*	$\lvert\mu_a\rvert$/ $\lvert\mu_b\rvert$/ $\lvert\mu_c\rvert$
I	0.0	34.2	20135/2243/2213	0.1/0.6/0.6	0.0	30.3	19637/2263/2237	0.1/0.8/0.6
II	1.1	21.8	10203/3061/2651	0.4/0.1/0.9	0.4	26.0	10008/3137/2695	0.3/0.0/1.0
III	2.0	15.5	14730/2703/2368	0.5/0.5/0.7	1.9	14.3	14636/2730/2386	0.5/0.6/0.8
IV	3.1	9.9	9612/3174/2700	0.5/0.3/0.7	2.5	11.0	9466/3247/2741	0.6/0.4/0.7
V	4.2	6.3	8842/3539/2937	0.8/0.8/0.4	3.3	7.9	8748/3613/2989	0.8/0.8/0.5
VI	5.0	4.5	13446/2637/2452	0.3/0.8/0.2	5.4	3.5	13089/2685/2492	0.4/0.9/0.2
VII	5.8	3.2	8654/3573/2916	0.5/0.4/0.2	5.6	3.2	8562/3648/2965	0.6/0.4/0.2
VIII	5.6	3.6	20847/2230/2177	0.4/0.1/1.0	5.7	3.0	20516/2246/2196	0.4/0.1/1.0
IX	9.2	0.8	13916/2627/2413	0.6/0.4/0.9	9.2	0.7	13388/2689/2463	0.6/0.3/1.0

Spectral analysis

According to the high-level quantum mechanical calculations in this work (Table 1), apart from the global minimum (conformer I), AMA has another four low-energy conformers (II–V) with ΔE_{ZPE} < 5.0 kJ mol^{-1} which possess non-zero electric dipole components and thus, should be observable by FTMW spectroscopy in a supersonic jet. The predicted rotational constants (*A*, *B*, and *C*) for each conformer are sufficiently unique so as to allow their unambiguous identification.

Transitions due to conformer I were readily identified in the broadband chirped pulse (cp) FTMW spectrum. Those were predominantly *b*- and *c*-type Q-branch transitions, lying in the upper limit of our cp-FTMW instrument around 17–18 GHz. Despite the small magnitude of the μ_a dipole (0.1 D), we were able to detect a few *a*-type rotational transitions for conformer I. Although the transitions due to conformer I dominated the spectrum, three additional sets of rotational transitions were observed in the survey spectrum (Figure 2A). The observed patterns were consistent with conformers II, III and V based on the supporting quantum chemical predictions. All assigned transitions were confirmed through measurements of their characteristic ^{14}N hyperfine structure using the Balle-Flygare (BF) FTMW instrument. Based on careful measurements using the cavity-based instrument and considering the calculated dipole moment components for each identified conformer, we estimate the experimental abundances of conformers I, II, III and V to be approximately 40%, 36%, 22% and 2%, respectively. This is a rough estimate as transitions with comparable quantum numbers for each conformer lie more than 2 GHz apart.

Interestingly, additional splittings were detected for some transitions with higher J rotational quantum number for conformer I. The splitting pattern (~1:1 ratio) is consistent with a tunneling motion associated with interconversion between two equivalent forms of I (I+ and I-) which would require internal motions of both the allyl and amino groups (Figure 3). A sample of the cavity-based spectrum, showing the F'–F = 3–2 ^{14}N hyperfine component and the tunneling splitting for the 2_{11}–2_{02} transition of conformer I, is provided in Figure 2B. For conformer III, although the $|\mu_c|$ component is calculated to be greater than the $|\mu_a|$ and $|\mu_b|$ components (Table 1), no *c*-type transitions were observed. This is likely caused by an inversion motion of the NH group that is symmetric along the *c*-axis perpendicular to the heavy atom backbone of AMA in Figure 1 which averages μ_c to zero if the ground state of III is above the barrier to this motion. A similar case has been reported in previous rotational spectroscopic studies of other amino containing compounds, such as 3-aminophenol.[23] Despite a careful search, transitions due to other conformers of AMA were not detected.

All measured rotational transitions were fitted with Pickett's SPFIT program[24] using Watson's A-reduced Hamiltonian in the I^r representation to yield experimental rotational, quartic centrifugal distortion and ^{14}N quadrupole coupling constants. The determined spectroscopic parameters for each conformer are provided in Table 2, while the complete line lists including individual hyperfine components and residuals are given as supplementary data (Tables S14–S17). The two tunneling states were fitted independently and are labeled in Table 2 as I+ and I-.

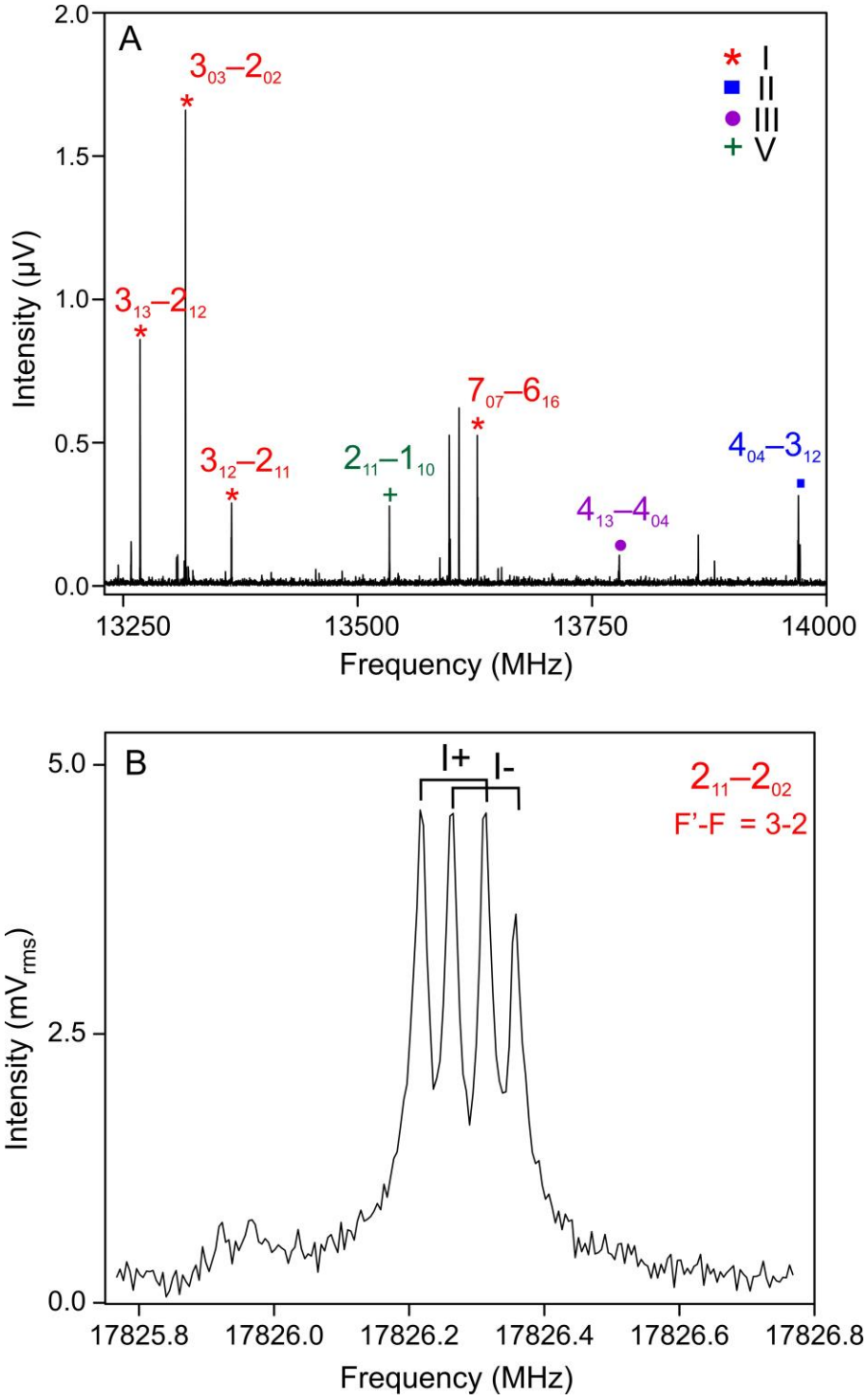

Figure 2. A) Sample of the broadband cp-FTMW spectrum (1.5 million FIDs) showing rotational transitions belonging to the parent species of conformers I, II, III and V. B) BF-FTMW spectrum (200 cycles) of the 2_{11}–2_{02} transition (F'-F = 3-2 hyperfine component) of conformer I highlighting the tunneling splitting.

Table 2. Experimental spectroscopic parameters for the four observed conformers of AMA

Parameter	I+	I-	II	III	V
A/MHz[a]	19998.1762(21)	19998.2173(20)	10173.23585(46)	14539.2746(48)	8773.1220(25)
B/MHz	2235.73639(58)	2235.73865(58)	3050.66194(22)	2699.7120(10)	3533.8400(17)
C/MHz	2203.14081(59)	2203.14302(58)	2641.63405(16)	2362.97445(96)	2932.5425(15)
Δ_J/kHz[b]	[0.63140769]	[0.63140769]	3.2139(80)	0.593(30)	3.337(50)
Δ_{JK}/kHz	-23.31(14)	-23.68(15)	-25.240(71)	-2.90(42)	-11.49(40)
Δ_K/kHz	[433.87203]	[433.87203]	[87.552397]	[36.947153]	[23.483135]
δ_J/kHz	[-0.090601327]	[-0.090601327]	0.9530(53)	[0.100861]	0.942(75)
δ_K/kHz	[40.889685]	[40.889685]	[5.0103483]	[1.20664]	[4.0555968]
1.5 (χ_{aa})/MHz[c]	4.3037(52)	4.3045(55)	3.7874(14)	3.707(11)	1.4243(82)
0.25 (χ_{bb}-χ_{cc})/MHz	-0.4038(24)	-0.3995(25)	1.87302(44)	0.7150(60)	0.2337(27)
$\mu_a/\mu_b/\mu_c$[d]	y/y/y	y/y/y	y/y/y	y/y/n	y/y/n
N[e]	111		60	27	21
σ/kHz[f]	6.4		1.4	5.8	3.2

[a]Rotational constants; [b]quartic centrifugal distortion constants; [c]^{14}N nuclear quadrupole coupling constants; [d]electric dipole moment components ("y" if observed and "n" if not observed); [e]total number of lines (*N*) in the fit; [f]root-mean-square deviation of the fit (σ). Values in brackets were fixed to the calculated values at B2PLYP-D3(BJ)/aug-cc-pVTZ. The full set of calculated constants are provided in Table S13. In table S14, the % deviation between the experimental and calculated rotational and ^{14}N quadrupole coupling constants for the three different levels of theory are provided.

Discussion

The conformational analysis of AMA by high-level quantum mechanical calculations and modern FTMW spectroscopy reveals a rich and competitive conformational behaviour for this seemingly simple molecule. From nine stable conformers (ΔE_{ZPE} < 10 kJ mol^{-1}, Table 1) predicted at 298K, four (I, II, III and V, Figure 1) were observed in the supersonic jet expansion. The previous assertion that conformer I is at least 3.0 kJ mol^{-1} more stable than any other rotamer of AMA[20] is inaccurate as supported by the observation of transitions from the four conformers whose intensities

are consistent with the calculated dipole moments and relative energies from both DFT and *ab initio* calculations—I (0.0 kJ mol^{-1}), II (~1.0 kJ mol^{-1}), III (2.0 kJ mol^{-1}) and V (~3.0–4.0 kJ mol^{-1}) in this work. As mentioned above, no transitions for conformers IV, VI, VII, VIII and IX were identified in the rotational spectrum. There are two common explanations invoked[25] to justify the absence of stable conformers in a molecular beam experiment: (1) the higher energy conformers are not abundant in the sample from the start and/or (2) they experience facile relaxation to lower energy forms through collisions with the carrier gas during the expansion.

At room temperature, conformers with relative energies higher than 5.0 kJ mol^{-1} (VI, VII, VIII and IX) are expected to be less than 6.0% populated based on the Boltzmann formula and, coupled with the dipole moment components in Table 1, are unlikely to be observed in the supersonic jet even if they are metastable. Nevertheless, to better characterize the conformational space of AMA, we considered relaxation pathways connecting the various conformers at both B2PLYP-D3(BJ)/aug-cc-pVTZ and MP2/aug-cc-pVTZ levels as shown in Figure S1. These are in essence cross sections of the full three-dimensional PES displayed in Figure 1. Considering the estimated energy barrier heights (Figure S1), relaxation from VIII→I (~4.0–5.0kJ mol^{-1}) and IX→II (~3.0 kJ mol^{-1}) is possible, while all the other conformers should be metastable as they correspond to deeper pockets on the PES. The non-observation of transitions of conformer IV is somewhat surprising based on its low relative energy (~2.5 – 3.1 kJ mol^{-1}) and electric dipole moment components (Table 1). Even though the calculations indicate that IV is metastable, there is still a possibility of conformational cooling from IV to II given their geometric similarities (Figure 1). The conformational relaxations of the above-mentioned

higher energy conformers into I and II are supported by their enriched conformational abundances of 40% and 36%, respectively, observed in the supersonic jet.

Interconversion pathways also provide useful insight into the tunnelling splitting observed for conformer I. The intensity ratio (Figure 2B) of the two components is consistent with tunnelling between two equivalent forms of I (I+ and I-, Figure 3) which requires motion of both the allyl and amino groups in the same direction. A possible tunneling trajectory, modeled in a sequential two-step fashion, is proposed in Figure 3. By starting with the amino inversion followed by the allyl torsion, or vice-versa, the lowest energy tunneling path requires passing through two transition states (TS). These are connected by an intermediate energy minimum structure (conformer VIII) in which the allyl group and the amino hydrogen point out of the molecular plane in opposite directions to each other. In the TS for the allyl torsion, the terminal double bond and the amino hydrogen are arranged in a way that minimizes steric repulsions, while in the TS for the amino inversion, these groups are spatially closer. This results in a lower barrier height for the allyl torsion compared to the NH inversion (Figure 3). Previous studies of related compounds, for example, have shown that a pathway involving changes in two geometric coordinates of a molecule can occur not only via two steps but also in a concerted way as proposed for the amine azetidine.[26,27] For conformer I, a concerted route would involve a planar TS geometry with C_s symmetry which is an unlikely pathway given the high estimated barrier of ~70.0 kJ mol^{-1} from B2PLYP-D3/aug-cc-pVTZ.

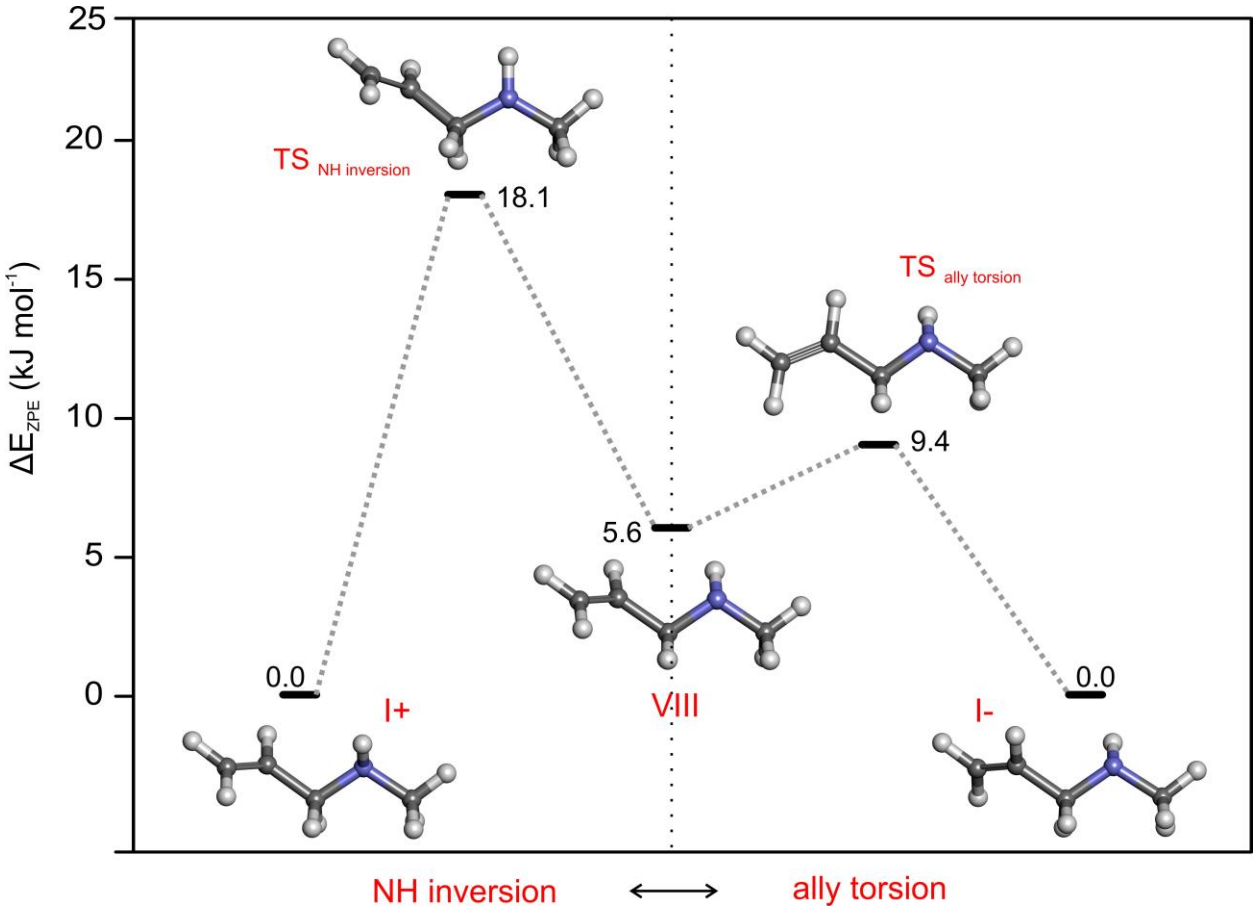

Figure 3. Possible two-step tunneling pathway for the interconversion between the equivalent forms of I obtained at the B2PLYP-D3(BJ)/aug-cc-pVTZ level of theory.

To identify possible non-covalent interactions that influence the conformer energy ordering of AMA, we used natural bond orbital and non-covalent interaction analyses. The results suggest a complex interplay of competing effects that stabilize and destabilize the individual conformers. The NCI analysis (Figure S2), for example, does not show any attractive or repulsive contacts in conformers I, V and VIII, but reveals weak CH···π attractive interactions in II, IV, VI and IX, CH···N in III and NH···π in VII. These contacts are seen by the blue-green regions on the isosurfaces between the atoms involved in the

interaction. It is worth noting that each of these contacts is accompanied by destabilizing repulsive effects (reddish part in the isosurfaces) of similar magnitude. Most importantly, the global minimum geometry is not stabilized by CH···π interactions suggesting that intramolecular hydrogen bonding is not the dominant factor governing the conformational behaviour of AMA as previously thought.[20]

NBO calculations (Table S19) also confirm the absence of a NH···π hydrogen bond in I, but do reveal that the arrangement of the allyl group and the amino hydrogen favors electron transfer from the lone-pair on nitrogen n_N into the antibonding π* and σ* orbitals of the C=C and C–C bonds, respectively. In fact, charge-transfer interactions involving the lone-pair at nitrogen and the vicinal methylene and methyl groups are observed for all nine conformers (Table S19). The magnitudes of the interactions vary depending on the geometric relationship between the lone-pair and the CH_2 and CH_3 moieties. The central role of hyperconjugation in stabilizing conformer I is apparent when comparing its interaction perturbation energies with those of conformer VIII which has a similar geometry but lacks both $n_N \rightarrow \pi^*_{C=C}$ and $n_N \rightarrow \sigma^*_{C-C}$ interactions due to the opposite disposition of the allyl and amino groups. The energy difference of ~5.0–6.0 kJ mol^{-1} between I and VIII is analogous to the sum of the second-order perturbation energies for the $n_N \rightarrow \pi^*_{C=C}$ and $n_N \rightarrow \sigma^*_{C-C}$ hyperconjugative interactions (~5.5 kJ mol^{-1}) observed in I. Although in other conformers the hyperconjugative interactions present similar or even larger values (Table S19), their geometries are also more destabilized by repulsive contacts as visualized from the NCI isosurfaces which makes them slightly less stable than I. The multifaceted conformational preferences of AMA can therefore be rationalized

in terms of a delicate balance of destabilization due to steric effects and stabilization from hyperconjugative interactions.

Conclusions

A detailed conformational study of AMA was completed using Fourier transform microwave spectroscopy and high-level quantum mechanical calculations. Rotational transitions for four stable conformers (I, II, III and V) were observed whose patterns agree with predictions from both DFT and *ab initio* calculations and show the characteristic hyperfine structure due to the ^{14}N quadrupolar nucleus. A two-step pathway is presented as the most energetically favourable route for the interconversion between the two equivalent forms of I (I+ and I-) to justify the observed tunneling splitting. The stable geometries of AMA are not governed by an isolated effect, but are rather the consequence of a tight competition between destabilizing steric effects and stabilizing hyperconjugative interactions as supported by the NCI and NBO calculations. This is the driving force behind the rich conformational landscape of AMA. The experimental and theoretical results presented here lay a critical foundation for further investigations of AMA and its decomposition products of atmospheric and astrochemical interest.

Experimental Methods

A commercially available sample of *N*-allylmethylamine (96% purity) was purchased from Alfa Aesar Canada and used without further purification. Given that the sample is a liquid at room temperature with a relatively low boiling point (61-62^{o}C), a gas mixture containing 1.0% of the title compound in neon (100 kPa) was prepared at room

temperature and expanded into the high vacuum chamber of the spectrometers using a pulsed nozzle (1 mm diameter orifice) to create a supersonic jet. The rotational spectrum of AMA was collected using a chirped pulse and a cavity-based Balle-Flygare type Fourier transform microwave spectrometer, which were described in detail previously.[28,29] Initially, the broadband cp-FTMW spectrum was recorded from 8–18 GHz in segments of 2 GHz from which the most intense rotational transitions due to different conformers of AMA were identified. Later, to collect transitions at higher frequencies and to resolve the hyperfine structure due to the ^{14}N quadrupolar nucleus, final frequency measurements were performed using the BF-FTMW instrument from 8–22 GHz which provides higher resolution and sensitivity. Rotational transitions recorded using the cavity-based spectrometer normally have line widths of ~7 kHz (FWHM) when the free induction decay is recorded for 400 μs allowing the uncertainty in the line positions to be determined to within $\pm$ 2 kHz. Due to the collinear arrangement of the molecular beam and the resonator axis in the BF-FTMW spectrometer, all rotational transitions collected using this instrument show a doublet splitting due to the Doppler effect.

Computational Methods

To identify the conformers of AMA, we initially performed a conformational search at the GFN2-xTB[30] level of theory using the Conformer-Rotamer Ensemble Sampling Tool (CREST) available in the extended tight binding (xTB) program package.[31,32] The conformational search identified 17 possible geometries of AMA. In the meantime, a three-dimensional potential energy surface was obtained by scanning the δ (C1=C2–C3–N) and θ (C2–C3–N–C4) dihedral angles simultaneously in 36 steps of 10º for each at

the B3LYP[33]-D3(BJ)[34,35]/cc-pVTZ[36] level. During the scan calculations, all other geometric parameters were allowed to relax. The resulting PES, shown in Figure 1, yielded nine unique energy minima. All of the 17 and nine geometries obtained from the aforementioned approaches were then fully optimized at higher levels of theory using the density-functional theory B3LYP[33]-D3(BJ)[34,35] and double-hybrid B2PLYP[37]-D3(BJ)[34,35] functionals along with the *ab initio* MP2[38] method. All optimizations were performed using Dunning's aug-cc-pVTZ basis sets.[36] Harmonic frequency calculations were also carried out to verify the nature of the stationary points. In the end, these calculations resulted in a total of nine true minima for AMA whose relative energies lie within an energy window of 10 kJ mol^{-1}.

Several relaxed potential energy curves were subsequently computed using both DFT and MP2 methods by varying the geometric coordinates of interest in steps of 10º to model possible interconversion and tunnelling pathways between minima. As needed, transition state structures were optimized and confirmed by the presence of a single imaginary frequency. All scan, optimization and harmonic frequency calculations were computed using the Gaussian 16 program.[39] The effects governing the conformational preferences of the observed conformers were subsequently evaluated using natural bond orbital [21] and non-covalent interaction[22] analyses carried out with the NBO 7.0[40] and NCIPLOT[41] programs, respectively.

Acknowledgements

The authors acknowledge the Natural Sciences and Engineering Research Council of Canada (NSERC) for research funding through the Discovery Grants program and the

University of Manitoba for its research computing facility (GREX). W.G.D.P.S and T.P. are grateful for financial support provided through a University of Manitoba Graduate Fellowship and the GETS program, respectively, subsidized by the Faculty of Graduate Studies.

Keywords: computational chemistry, conformational analysis, hyperconjugation, rotational spectroscopy

References

[1] X. Ge, A. S. Wexler, S. L. Clegg, *Atmos. Environ.* **2011**, *45*, 524–546.

[2] B. A. McGuire, *Astrophys. J. Suppl. Ser.* **2018**, *239*, 17.

[3] S. L. Miller, *Science* **1953**, *117*, 528–529.

[4] P. D. Holtom, C. J. Bennett, Y. Osamura, N. J. Mason, R. I. Kaiser, *Astrophys. J.* **2005**, *626*, 940–952.

[5] A. Belloche, K. M. Menten, C. Comito, H. S. P. Müller, P. Schilke, J. Ott, S. Thorwirth, C. Hieret, *Astron. Astrophys.* **2008**, *482*, 179–196.

[6] N. Kaifu, M. Morimoto, K. Nagane, K. Akabane, T. Iguchi, K. Takagi, *Astrophys. J.* **1974**, *191*, L135.

[7] N. Fourikis, K. Takagi, M. Morimoto, *Astrophys. J.* **1974**, *191*, L139.

[8] P. Vitins, K. W. Egger, *J. Chem. Soc., Perkin Trans. 2* **1974**, 1289–1291.

[9] A. R. Oliaey, A. Shiroudi, E. Zahedi, M. S. Deleuze, *Monatshefte für Chemie - Chem. Mon.* **2018**, *149*, 1389–1400.

[10] N. Marcelino, J. Cernicharo, M. Agúndez, E. Roueff, M. Gerin, J. Martín-Pintado, R. Mauersberger, C. Thum, *Astrophys. J.* **2007**, *665*, L127–L130.

[11] P. D. Godfrey, R. D. Brown, B. J. Robinson, M. W. Sinclair, *Astrophys. Lett.* **1973**, *13*, 119.

[12] W. Sun, O. P. Sogeke, W. G. D. P. Silva, J. van Wijngaarden, *J. Chem. Phys.* **2019**, *151*, 194304.

[13] J. Stitsky, W. G. D. P. Silva, W. Sun, J. van Wijngaarden, *J. Phys. Chem. A* **2020**, *124*, 3876–3885.

[14] B. Galabov, S. Kim, Y. Xie, H. F. Schaefer, M. L. Leininger, J. R. Durig, *J. Phys. Chem. A* **2008**, *112*, 2120–2124.

[15] W. A. Herrebout, C. Zheng, B. J. van der Veken, J. R. Durig, *J. Mol. Struct.* **2003**, *645*, 109–132.

[16] I. Botskor, H. D. Rudolph, G. Roussy, *J. Mol. Spectrosc.* **1974**, *53*, 15–36.

[17] I. Botskor, H. D. Rudolph, G. Roussy, *J. Mol. Spectrosc.* **1974**, *52*, 457–484.

[18] G. Roussy, J. Demaison, I. Botskor, H. D. Rudolph, *J. Mol. Spectrosc.* **1971**, *38*, 535–544.

[19] I. Botskor, H. D. Rudolph, *J. Mol. Spectrosc.* **1978**, *71*, 430–445.

[20] K.-M. Marstokk, H. Møllendal, *Acta Chem. Scand.* **1986**, *40a*, 615–621.

[21] F. Weinhold, C. R. Landis, E. D. Glendening, *Int. Rev. Phys. Chem.* **2016**, *35*, 399–440.

[22] E. R. Johnson, S. Keinan, P. Mori-Sánchez, J. Contreras-García, A. J. Cohen, W. Yang, *J. Am. Chem. Soc.* **2010**, *132*, 6498–6506.

[23] F. Filsinger, K. Wohlfart, M. Schnell, J.-U. Grabow, *Phys. Chem. Chem. Phys.* **2008**, *10*, 666–673.

[24] Z. Kisiel, "PROSPE - Programs for ROtational SPEctroscopy," can be found under http://www.ifpan.edu.pl/~kisiel/prospe.htm.

[25] D. Loru, M. M. Quesada-Moreno, J. R. Avilés-Moreno, N. Jarman, T. R. Huet, J. J. López-González, M. E. Sanz, *ChemPhysChem* **2017**, *18*, 274–280.

[26] J. C. López, S. Blanco, A. Lesarri, J. L. Alonso, *J. Chem. Phys.* **2001**, *114*, 2237–2250.

[27] S. R. Domingos, C. Pérez, C. Medcraft, P. Pinacho, M. Schnell, *Phys. Chem. Chem. Phys.* **2016**, *18*, 16682–16689.

[28] L. Evangelisti, G. Sedo, J. van Wijngaarden, *J. Phys. Chem. A* **2011**, *115*, 685–690.

[29] G. Sedo, J. van Wijngaarden, *J. Chem. Phys.* **2009**, *131*, 044303.

[30] C. Bannwarth, S. Ehlert, S. Grimme, *J. Chem. Theory Comput.* **2019**, *15*, 1652–1671.

[31] S. Grimme, *J. Chem. Theory Comput.* **2019**, *15*, 2847–2862.

[32] P. Pracht, F. Bohle, S. Grimme, *Phys. Chem. Chem. Phys.* **2020**, *22*, 7169–7192.

[33] A. D. Becke, *J. Chem. Phys.* **1993**, *98*, 5648–5652.

[34] S. Grimme, S. Ehrlich, L. Goerigk, *J. Comput. Chem.* **2011**, *32*, 1456–1465.

[35] S. Grimme, J. Antony, S. Ehrlich, H. Krieg, *J. Chem. Phys.* **2010**, *132*, 154104.

[36] T. H. Dunning, *J. Chem. Phys.* **1989**, *90*, 1007–1023.

[37] S. Grimme, *J. Chem. Phys.* **2006**, *124*, 034108.

[38] C. Møller, M. S. Plesset, *Phys. Rev.* **1934**, *46*, 618–622.

[39] M. J. Frisch, G. W. Trucks, H. B. Schlegel, G. E. Scuseria, M. A. Robb, J. R. Cheeseman, G. Scalmani, V. Barone, B. Mennucci, G. A. Petersson, et al., Gaussian 16 Revision C.01, Gaussian Inc., Wallingford CT (United States), **2010**.

[40] E. D. Glendening, J. K. Badenhoop, A. E. Reed, J. E. Carpenter, J. A. Bohmann, C. M. Morales, P. Karafiloglou, C. R. Landis, F. Weinhold, C. R. Landis, NBO 7.0, Theoretical Chemistry Institute, University of Wisconsin, Madison (United States), **2018**.

[41] J. Contreras-García, E. R. Johnson, S. Keinan, R. Chaudret, J.-P. Piquemal, D. N. Beratan, W. Yang, *J. Chem. Theory Comput.* **2011**, *7*, 625–632.

Table of Contents

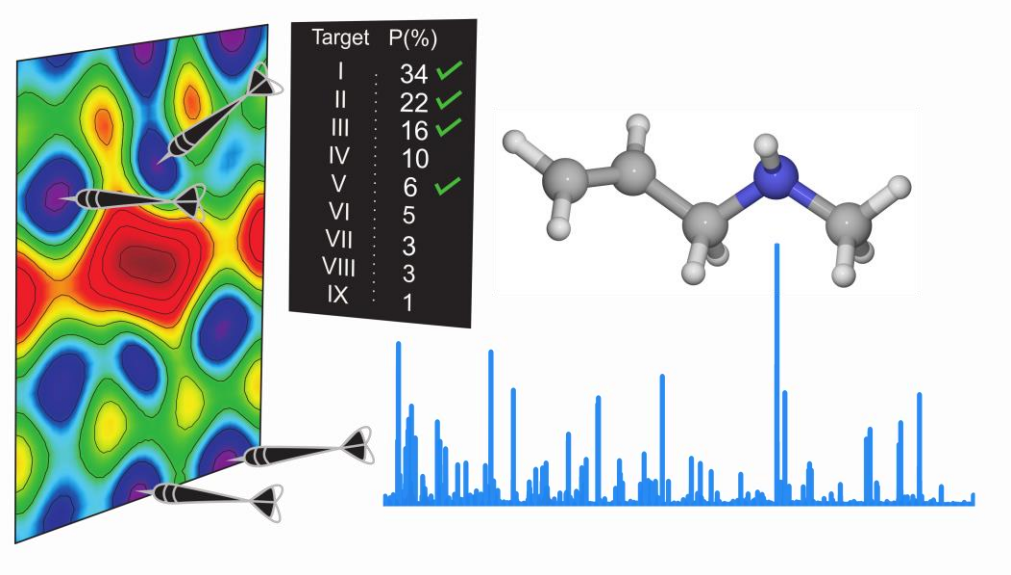

The conformers of *N*-allylmethylamine: Four conformers were observed by their rotational signatures using microwave spectroscopy combined with quantum chemical calculations. Their relative energy orderings are explained by a highly competitive interplay between steric hindrance and hyperconjugative interactions.